

Improved calculation of the second-order ocean Doppler spectrum for sea state inversion

Charles-Antoine Gu erin (MIO, Univ Toulon, Aix-Marseille Univ, CNRS, IRD, Toulon, France)

Abstract—We propose a simple method, based on an original change of variables, for the fast and accurate calculation of the second-order ocean Doppler spectrum that describes the sea echo of High-Frequency radars. A byproduct of the technique is the derivation of an improved weighting function which can be used for the inversion of the main sea state parameters. For this we revisit Barrick’s method for the estimation of the significant wave height and the mean period from the ocean Doppler spectrum. On the basis of numerical simulations we show that a better estimation of these parameters can be reached but necessitates a preliminary bias correction that depends only on the radar frequency. A second consequence of our formulation is the derivation of a simple yet analytical nonlinear approximation of the second-order ocean Doppler spectrum when the Doppler frequency is larger than the Bragg frequency. This opens new perspective for the inversion of directional wave spectra from High-Frequency radar measurements.

Index Terms—High-Frequency radar, Doppler spectrum, sea state inversion

I. INTRODUCTION

High-Frequency radars have been used for half a century as an efficient tool for measuring surface currents and waves in the coastal region (see e.g. [1] for a recent review). In this range of radio frequencies (3-30 MHz), the backscattered Doppler spectrum from the sea surface is accurately described by the second-order electromagnetic and hydrodynamic perturbation theory, whose complete equations were published by Barrick half a century ago [2]. Hasselmann [3] first suggested that the continuous component of the ocean Doppler spectrum is essentially a replica of the ocean wave spectrum translated by the Bragg frequency and thus could be used for sea state inversion. As many followers have shown, this is only a coarse approximation and estimating the wavenumber spectrum has both mathematical and practical limitations (e.g. [4]). There is no unique relationship between the ocean spectrum and the Doppler spectrum, so that the inversion can only be performed with some additional constraints. The numerical inversion of the Doppler spectrum, using either Barrick’s linearized equations [5], [6] or their fully nonlinear expression [7], is computationally intensive. It requires solving a large number of direct problems involving the tricky calculation of a double integral with singular kernel and constrained variables. In this paper, we propose an improved method for the fast and accurate calculation of the second-order ocean Doppler spectrum based on an appropriate, original change of variables (section II). For technical reasons we limit this analysis to the backscattering configuration and to the deep-water gravity wave dispersion relation for the hydrodynamic processes at play, a double assumption which corresponds to the majority of practical situations. Equipped with this new formulation,

we address the classical problem of estimating the main sea state parameters from the integral properties of the Doppler spectrum, following the method first proposed by Barrick [8], [9]. To do this, we introduce a function, referred to as the “Zeta” function, which has the same structure as the second-order Doppler spectrum but is free of the coupling coefficient. We show that the Zeta function can, in principle, be used for the estimation of the significant wave height (SWH) and the mean period. However, numerical simulations using a typical ocean wave spectrum model show that the estimation of these 2 parameters must be corrected by a frequency-dependent multiplicative and additive bias, respectively (section III). Transferring these results to the actual Doppler spectrum requires the use of a weighting function, as first proposed by Barrick, to account for the influence of the coupling coefficient. In the light of our improved formulation we derive a new weighting function (Section IV) to approximate the Zeta function, resulting in a more accurate estimation of the sea state parameters. Our last result concerns the direct estimation of the ocean wave spectrum. For Doppler frequencies higher than the Bragg frequency we obtain, as a consequence of the new integral formulation, a simple analytical approximation which is verified to be extremely accurate (Section V).

II. EVALUATION OF THE SECOND-ORDER SPECTRUM

We consider the classical idealized problem of a High-Frequency radar measuring the backscattered ocean Doppler spectrum in vertical polarization at grazing incidence in the limit of an infinite sea surface patch. We denote f_0 the radar frequency, $k_0 = 2\pi f_0/c_0$ the associated electromagnetic wavenumber, where $c_0 = 3.10^8$ m/s is the speed of light in vacuum, and \mathbf{k}_0 the horizontal electromagnetic wave vector of the incident electric field. As it is well known in ocean radar remote sensing, the so-called Bragg wave vector $\mathbf{k}_B = -2\mathbf{k}_0$, Bragg wavenumber $k_B = 2k_0$ and Bragg frequency $\omega_B = \sqrt{gk_B}$ play a prominent role in the expression of the backscattered field. The complete expression of the ocean Doppler cross-section appeared for the first time in [2]. It is given by a sum of two terms, $\sigma(\omega) = \sigma_1(\omega) + \sigma_2(\omega)$, where σ_1 contains the first-order Bragg peaks

$$\sigma_1(\omega) = \mathcal{N} \sum_{n_1=\pm 1} S_d(n_1 \mathbf{k}_B) \delta(\omega - \omega_B) \quad (1)$$

and σ_2 is a second-order, continuous component

$$\begin{aligned} \sigma_2(\omega) = \mathcal{N} \sum_{n_1=\pm 1} \sum_{n_2=\pm 1} \int S_d(n_1 \mathbf{k}_1) S_d(n_2 \mathbf{k}_2) \\ \times |\Gamma|^2 \delta(\omega - n_1 \omega_1 - n_2 \omega_2) d\mathbf{k}_1 \end{aligned} \quad (2)$$

where $\mathcal{N} = 2^6 \pi K_0^4$ is a normalization constant and $S_d(\mathbf{k})$ the directional ocean spectrum. The wave vectors entering in this integral are related by the Bragg resonance condition and the associated frequencies are given by the deep water gravity waves dispersion relation

$$\mathbf{k}_1 + \mathbf{k}_2 = \mathbf{k}_B, \quad \omega_1 = \sqrt{gk_1}, \quad \omega_2 = \sqrt{gk_2} \quad (3)$$

where $g = 9.81 \text{ m s}^{-2}$ is the gravity constant. The kernel Γ can be decomposed into a hydrodynamic kernel Γ_H and an EM kernel Γ_{EM}

$$\Gamma(\mathbf{k}_1, \mathbf{k}_2, \omega, \omega_B) = \Gamma_H + \Gamma_{EM} \quad (4)$$

with

$$\Gamma_H = -\frac{i}{2} \left(k_1 + k_2 - \frac{(k_1 k_2 - \mathbf{k}_1 \cdot \mathbf{k}_2)(\omega^2 + \omega_B^2)}{n_1 n_2 \sqrt{k_1 k_2}(\omega^2 - \omega_B^2)} \right) \quad (5)$$

and

$$\Gamma_{EM} = \frac{1}{2} \frac{(\mathbf{k}_1 \cdot \mathbf{k}_B)(\mathbf{k}_2 \cdot \mathbf{k}_B) - 2\mathbf{k}_1 \cdot \mathbf{k}_2}{\sqrt{\mathbf{k}_1 \cdot \mathbf{k}_2} - \Delta/2} \quad (6)$$

where $\Delta = 0.011 - 0.012i$ is an impedance term that takes into account the finite conductivity of the sea surface in the High-Frequency domain. Each of the four components in (2) corresponding to the different sign combinations (n_1, n_2) addresses a different frequency domain of the Doppler spectrum. The combined geometrical constraints $\omega = n_1 \omega_1 + n_2 \omega_2$ and $\mathbf{k}_1 + \mathbf{k}_2 = \mathbf{k}_B$ impose $n_1 = n_2 = 1$ if $\omega \geq \omega_B$, $n_1 = n_2 = -1$ if $\omega \leq -\omega_B$ and $n_1 = -n_2 = \pm 1$ if $|\omega| \leq \omega_B$. The different combinations of signs thus cover the four distinct regions delimited by the first order Bragg lines.

The evaluation of the second-order integral (2) is difficult due to the delta function constraint with respect to the ω_1 and ω_2 variables, which has been analyzed in detail in [10]. For a prescribed value of ω , the admissible values of \mathbf{k}_1 follow closed contour lines in the (k_{1x}, k_{1y}) plane. The contours have 2 disjoint components for $\omega < \sqrt{2}\omega_B$ that merge into a single one for $\omega > \sqrt{2}\omega_B$. The intensification of the contour lines at the transition produces a singularity of the function $\sigma_2(\omega)$ at $\omega = \sqrt{2}\omega_B$. A second singularity is caused by the EM kernel, that has a sharp maximum for $\mathbf{k}_1 \cdot \mathbf{k}_2 = 0$ (this would be a mathematical singularity without the finite impedance term). The locus of this singularity is a circle which is found tangential to the contour line $\omega = 2^{3/4} \simeq 1.68\omega_B$; this results in a secondary, sharp maximum at this frequency. Considering the finite integration time T_i and the resulting finite frequency resolution $\Delta\omega = 2\pi/T_i$, the theoretical Doppler spectrum is actually smeared by some function $\Phi(\omega)$ of width $\Delta\omega$ [11]. This amounts to replace the Dirac function $\delta(\omega - n_1\omega_1 - n_2\omega_2)$ in the integrand of (2) by $\Phi(\omega - n_1\omega_1 - n_2\omega_2)$ where the integration domain is now two-dimensional with no further constraint on the integration variable \mathbf{k}_1 . This allows for a straightforward computation of σ_2 but requires a tight 2D sampling of the k-space that is numerically not efficient. An alternative computation can be obtained by reducing the two-dimensional integral (2) to a single one by eliminating the delta function through an appropriate change of variables. The standard way to do this [10] is to use polar coordinates (k_1, θ) for the wave vector \mathbf{k}_1 and to operate a change a variable $(k_1, \theta) \rightarrow (\omega_1 + \omega_2, \theta)$. However, the change of variable is only

implicit and requires an extra numerical inversion for each value of ω to calculate the new integrand. We here propose an alternative change of variable that is more efficient and fully explicit. It works only with deep water gravity waves, which follow the simple dispersion relation $\omega^2 = gk$. This is, however, the case of main interest for HF radars. To simplify the calculation we use reduced frequencies and wave numbers

$$\begin{aligned} \kappa_1 &= \mathbf{k}_1/k_B, \quad \kappa_2 = \mathbf{k}_2/k_B, \quad \kappa_B = \mathbf{k}_B/k_B, \\ \nu_1 &= \omega_1/\omega_B, \quad \nu_2 = \omega_2/\omega_B, \quad \nu = \omega/\omega_B. \end{aligned} \quad (7)$$

This is relevant because the kernel Γ depends only on the reduced variables and the Bragg wavenumber

$$\Gamma(\mathbf{k}_1, \mathbf{k}_2, \omega, \omega_B) = k_B \Gamma(\kappa_1, \kappa_2, \nu, 1). \quad (8)$$

Assuming the reduced Bragg wave vector to be along the x-axis ($\kappa_B = (1, 0)$) we operate the change of variables

$$(\kappa_{1x}, \kappa_{1y}) \rightarrow (\nu_1, \nu_2). \quad (9)$$

Note that we thus replace the two-dimensional wave vector κ_1 by a set of 2 positive frequencies with the obvious advantage that these appear as the argument of the delta function in the integrand. On the upper half-space $\kappa_{1y} \geq 0$ we can

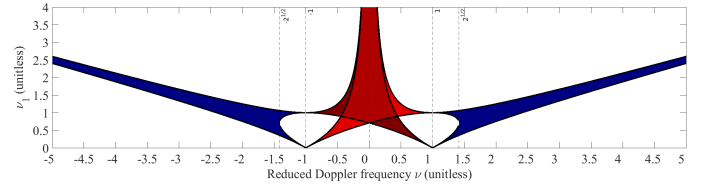


Fig. 1. Admissible values of the reduced frequency ν_1 seen in the (ν, ν_1) plane. For $|\nu| > 1$, the integration domain of the integral (12) corresponds to vertical cuts of the blue strips. For $|\nu| < 1$, the integration domains of the integrals (19) are given by vertical cuts of the dark red $(I_{-1,1})$ and light red $(I_{1,-1})$ regions.

derive a simple one-to-one relationship between old and new integration variables

$$\begin{aligned} \kappa_{1x}(\nu_1, \nu_2) &= \frac{1}{2} (1 + \nu_1^4 - \nu_2^4) \\ \kappa_{1y}(\nu_1, \nu_2) &= \left| \nu_1^4 - \frac{1}{4} (1 + \nu_1^4 - \nu_2^4)^2 \right|^{1/2} \end{aligned} \quad (10)$$

and the same holds on the lower half-space by changing the sign of κ_{1y} in (10). The Jacobian of the transformation is found to be

$$J(\nu_1, \nu_2) = \left| \frac{4\nu_1^3 \nu_2^3}{\kappa_{1y}(\nu_1, \nu_2)} \right|. \quad (11)$$

We now evaluate the second-order Doppler spectrum in this new set of variables by treating separately the frequency intervals between and outside the Bragg lines.

a) *Case $\omega > \omega_B$ ($n_1 = n_2 = 1$) or $\omega < -\omega_B$ ($n_1 = n_2 = -1$):* By separating the integrals over the two half-spaces and performing the integration over the ν_2 variable to eliminate the delta function we obtain

$$\sigma_2(\omega) = \mathcal{N} k_B^4 \omega_B^{-1} \int_{I(\nu)} \mathcal{S}(\nu_1) \gamma(\nu_1) \mathcal{J}(\nu_1) d\nu_1 \quad (12)$$

where γ is the reduced kernel expressed as a function of the sole reduced frequencies $\nu = \omega/\omega_B$ and ν_1

$$\gamma(\nu_1) = |\Gamma(\boldsymbol{\kappa}_1^+, \boldsymbol{\kappa}_2^+, \nu, 1)|^2 = |\Gamma(\boldsymbol{\kappa}_1^-, \boldsymbol{\kappa}_2^-, \nu, 1)|^2, \quad (13)$$

$\boldsymbol{\kappa}_1^\pm, \boldsymbol{\kappa}_2^\pm$ are the reduced wave vectors in the upper/lower half-space

$$\begin{aligned} \boldsymbol{\kappa}_1^\pm &= (\kappa_{1x}(\nu_1, |\nu| - \nu_1), \pm \kappa_{1y}(\nu_1, |\nu| - \nu_1)) \\ \boldsymbol{\kappa}_2^\pm &= (1 - \kappa_{1x}(\nu_1, |\nu| - \nu_1), \mp \kappa_{1y}(\nu_1, |\nu| - \nu_1)), \end{aligned} \quad (14)$$

\mathcal{S} is the corresponding product of directional ocean spectra

$$\mathcal{S}(\nu_1) = S_d(n_1 k_B \boldsymbol{\kappa}_1^+) S_d(n_1 k_B \boldsymbol{\kappa}_2^+) + S_d(n_1 k_B \boldsymbol{\kappa}_1^-) S_d(n_1 k_B \boldsymbol{\kappa}_2^-) \quad (15)$$

and \mathcal{J} is the Jacobian in the reduced frequency variable:

$$\mathcal{J} = J(\nu_1, |\nu| - \nu_1). \quad (16)$$

The integration domain $I(\nu)$ is a subset of the positive axis. It is limited to the values of ν_1 for which $\nu_2 \geq 0$ and for which the argument of the square root in (10) is positive, that is

$$\nu_1^4 - \frac{1}{4} (1 + \nu_1^4 - (|\nu| - \nu_1)^4)^2 \geq 0. \quad (17)$$

The limits of the domain can easily be identified analytically with the roots of the above equation. The integration domain $I(\nu)$ is composed of one or two disjoint intervals depending on the value of ν

$$\begin{aligned} &\left[\frac{\nu^2 - 1}{2|\nu|}, \frac{|\nu| - \sqrt{2 - \nu^2}}{2} \right] \cup \left[\frac{|\nu| + \sqrt{2 - \nu^2}}{2}, \frac{1 + \nu^2}{2|\nu|} \right], & 1 \leq |\nu| \leq \sqrt{2}, \\ &\left[\frac{\nu^2 - 1}{2|\nu|}, \frac{\nu^2 + 1}{2|\nu|} \right], & |\nu| > \sqrt{2}. \end{aligned} \quad (18)$$

Note that the integration domain is splitted in two disjoint intervals for $1 < |\nu| < \sqrt{2}$. However, these two intervals are interchanged by the transformation $\nu_1 \mapsto \nu_1 - \nu$. Since this transformation amounts to swap ν_1 and ν_2 in the integrand, this leaves γ , \mathcal{J} and \mathcal{S} unchanged. It follows that the 2 integrals on the lower and upper interval are identical so that it suffices to calculate one of them and multiply the result by two.

b) Case $|\omega| < \omega_B$ ($n_1 = -n_2 = \pm 1$): Similar calculations lead to the following expression for the second-order Doppler spectrum inside the Bragg lines:

$$\sigma_2(\omega) = \mathcal{N} k_B^4 \omega_B^{-1} \left\{ \int_{I_{1,-1}(\nu)} + \int_{I_{-1,1}(\nu)} \right\} \mathcal{S}(\nu_1) \gamma(\nu_1) \mathcal{J}(\nu_1) d\nu_1 \quad (19)$$

with the following adaptation of the integrand. On the interval $I_{1,-1}(\nu)$, the variable $|\nu| - \nu_1$ should be replaced by $\nu_1 - \nu$ in s (14) and (16), and (15) should be replaced by:

$$\mathcal{S}(\nu_1) = S_d(k_B \boldsymbol{\kappa}_1^+) S_d(-k_B \boldsymbol{\kappa}_2^+) + S_d(k_B \boldsymbol{\kappa}_1^-) S_d(-k_B \boldsymbol{\kappa}_2^-). \quad (20)$$

On the interval $I_{-1,1}(\nu)$, the variable $|\nu| - \nu_1$ should be replaced by $\nu_1 + \nu$ in s (14) and (16), and (15) should be replaced by

$$\mathcal{S}(\nu_1) = S_d(-k_B \boldsymbol{\kappa}_1^+) S_d(k_B \boldsymbol{\kappa}_2^+) + S_d(-k_B \boldsymbol{\kappa}_1^-) S_d(k_B \boldsymbol{\kappa}_2^-). \quad (21)$$

The integration domain $I_{1,-1}(\nu)$ is constrained by the conditions

$$\nu_1^4 - \frac{1}{4} (1 + \nu_1^4 - (\nu - \nu_1)^4)^2 \geq 0, \quad \nu_1 \geq \nu \quad (22)$$

leading to

$$I_{1,-1}(\nu) = \left[\frac{\nu + \sqrt{2 - \nu^2}}{2}, \frac{1 + \text{sign}(\nu)\nu^2}{2|\nu|} \right]. \quad (23)$$

Likewise the integration domain $I_{-1,1}(\nu)$ is constrained by the conditions

$$\nu_1^4 - \frac{1}{4} (1 + \nu_1^4 - (\nu + \nu_1)^4)^2 \geq 0, \quad \nu_1 \geq -\nu \quad (24)$$

leading to

$$I_{-1,1}(\nu) = \left[\frac{-\nu + \sqrt{2 - \nu^2}}{2}, \frac{1 - \text{sign}(\nu)\nu^2}{2|\nu|} \right]. \quad (25)$$

The complete integration domain defined by the union of $I(\nu)$ (for $|\nu| \geq 1$), $I_{1,-1}(\nu)$ and $I_{-1,1}(\nu)$ (for $|\nu| < 1$) is shown in the (ν, ν_1) plane in Fig. 1. Note that the transformation $\nu_1 \mapsto \nu_1 - \nu$ maps the interval $I_{1,-1}(\nu)$ to $I_{-1,1}(\nu)$. Again, since this transformation amounts to swap ν_1 and ν_2 in the integrand, this leaves γ and \mathcal{J} unchanged in the integral and transforms (20) to (21). It follows that the 2 integrals in (19) are identical so that it suffices to calculate one of them

$$\sigma_2(\omega) = 2\mathcal{N} k_B^4 \omega_B^{-1} \int_{I_{-1,1}(\nu)} \mathcal{S}(\nu_1) \gamma(\nu_1) \mathcal{J}(\nu_1) d\nu_1. \quad (26)$$

When ν_1 approaches the border of the domain, corresponding to one end of the intervals $I(\nu)$, $I_{1,-1}(\nu)$ or $I_{-1,1}(\nu)$, the Jacobian term $\mathcal{J}(\nu_1)$ has an integrable $1/\sqrt{\epsilon}$ singularity, except at the particular values $\nu = \pm\sqrt{2}$, where its denominator has a double root causing a non-integrable $1/\epsilon$ singularity. This recovers the result established in [12] that the Doppler spectrum has a logarithmic singularity at $\nu = \pm\sqrt{2}$. Apart from these 2 specific points, the singularity of the Jacobian at the borders of the domain can be handled properly by using the Gauss-Jabobi quadrature rule for numerical integration. We recall that

$$\int_{-1}^{+1} (x-1)^{-1/2} (x+1)^{-1/2} f(x) dx \simeq \sum_1^N w_j f(x_j) \quad (27)$$

where the nodes of the quadrature x_j are the zeros of the Jacobi polynomials and w_j the associated weights, the approximation being exact whenever f is constant. Many open source numerical routines can be found on the internet. This allows a fast and accurate calculation of the second-order ocean Doppler spectrum (12) at the cost of an ordinary one-dimensional integral.

The sea state dependence in the expression of the second-order Doppler spectrum enters through the ocean wave spectrum. Following the standard representation we write the directional wave spectrum in the form

$$S_d(\mathbf{k}) = k^{-1} S_o(k) D(k, \theta) \quad (28)$$

where $S_o(k)$ is the omnidirectional spectrum and $D(\theta)$ is an angular spreading function with the normalization $\int_0^{2\pi} D(\theta) d\theta = 1$ and the angle θ is measured with respect to the radar beam. It can also be expressed in term of the classical

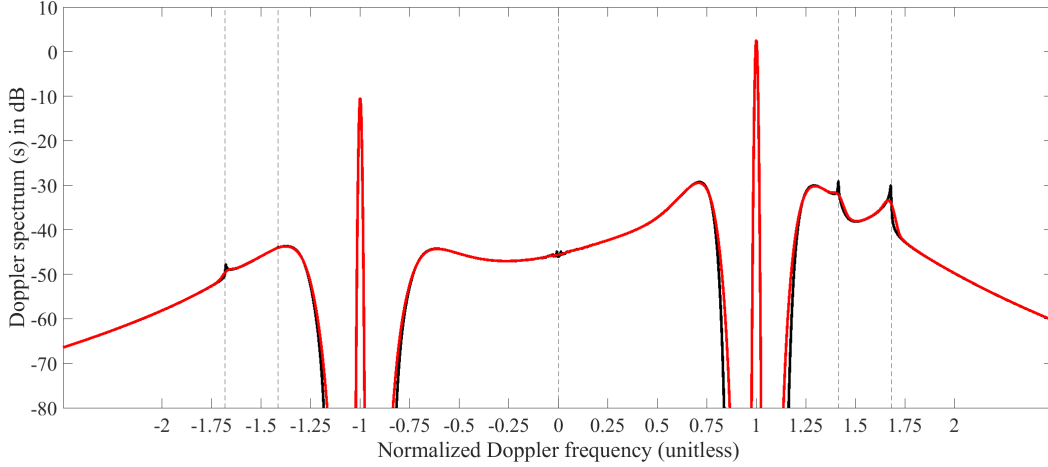


Fig. 2. Second-order Doppler spectrum at radar frequency $f_0 = 16$ MHz calculated with the improved formulation (12) as a function of the reduced Doppler frequency $\nu = \omega/\omega_B$. The ocean wave spectrum is a directional PM spectrum at 10 m/s wind speed with the radar looking upwind (black solid lines). Also shown is a smoothed Doppler spectrum corresponding to a finite frequency resolution of 0.01 Hz (red solid lines). The black dashed vertical lines mark the $\pm 2^{1/2}$ and $\pm 2^{3/4}$ singularities.

frequency spectrum $S_f(\omega)$ (using $S_o(k) = S_f(\omega)d\omega/dk$ and $\omega = \sqrt{gk}$)

$$S_d(\mathbf{k}) = \frac{1}{2}g^2\omega^{-3}S_f(\omega)D(\omega, \theta). \quad (29)$$

For the numerical simulations we have employed the classical Pierson-Moskowitz (PM) frequency spectrum

$$S_f(\omega) = Ag^2\omega^{-5}\exp(-B(g/U_{10}\omega)^4) \quad (30)$$

corresponding to an omnidirectional wavenumber spectrum

$$S_o(k) = \frac{A}{2}k^{-3}\exp(-Bg^2/(U_{10}^4k^2)) \quad (31)$$

where $A = 0.0081$, $B = 0.74$, U_{10} is the wind speed at 10 meter above the sea surface. For the angular spreading function we chose the classical cardioid shaped spreading function

$$D(\theta) = \alpha(\epsilon + (1 - \epsilon)\cos^4((\theta - \theta_w)/2)) \quad (32)$$

where α is the normalization constant, θ_w is the direction of wind with respect to the radar beam ($\theta_w = 0$ upwind) and $\epsilon = 0.05$ is a small parameter that allows to have a fraction of waves propagating against the wind, as it is often observed. An example of the resulting computation for the upwind ocean Doppler spectrum at wind speed $U_{10} = 10$ m/s is shown in Fig. 2 at the commonly used radar frequency $f_0 = 16$ MHz. We superimposed the smoothed version of this spectrum, which removes the delta-like singularity at $\omega = \pm\omega_B$ and the logarithmic singularity at $\omega = \pm\sqrt{2}\omega_B$ and corresponds to a practical situation. The computation was assessed by comparison (not shown here) with the aforementioned direct method based on a two-dimensional integration in the \mathbf{k}_1 space using a finite filter Φ instead of a Dirac function.

III. THE ZETA FUNCTION

We now consider the following function, henceforth referred to as the ‘‘Zeta function’’, obtained by removing the coupling

coefficient from the expression of the second-order ocean Doppler spectrum and replacing it with k_B^2 to keep the same dimension

$$\zeta(\omega) = \mathcal{N}k_B^2 \sum_{n_1=\pm 1} \sum_{n_2=\pm 1} \int S_d(n_1\mathbf{k}_1)S_d(n_2\mathbf{k}_2) \times \delta(\omega - n_1\omega_1 - n_2\omega_2)d\mathbf{k}_1. \quad (33)$$

As first suggested in [9], the main parameters of the ocean wave spectrum can be estimated with the first two moments of the Zeta function and we will follow the same argumentation. We first integrate the Zeta function over the frequency variable to get rid of the delta function in the integrand of ζ . The second step of the demonstration is obtained by noting that the ocean wave spectrum has a dominant value near the peak wavenumber $k_p \ll k_B$ so that its leading contribution can be extracted from the integral. This occurs when one of the variable \mathbf{k}_1 or \mathbf{k}_2 in the integrand is close to zero, leading in the end to

$$\int_{-\infty}^{+\infty} \zeta(\omega)d\omega \simeq 4\mathcal{N}k_B^2 \sum_{n_1=\pm 1} S_d(n_1\mathbf{k}_B) \int S_d(\mathbf{k})d\mathbf{k}. \quad (34)$$

The integral of the right-hand side is the variance of wave elevations

$$H_0^2 = \int S_d(\mathbf{k})d\mathbf{k} \quad (35)$$

while the discrete summation is the integral of the first-order Bragg peaks. Hence the Significant Wave Height (SWH) $H_s = 4H_0$ can be recovered from the Zeta function

$$H_s^2 = \frac{4 \int_{-\infty}^{+\infty} \zeta(\omega)d\omega}{k_B^2 \int_{-\infty}^{+\infty} \sigma_1(\omega)d\omega}. \quad (36)$$

To estimate the mean wave frequency we consider the positive frequency side of the Zeta function spectrum (assuming it

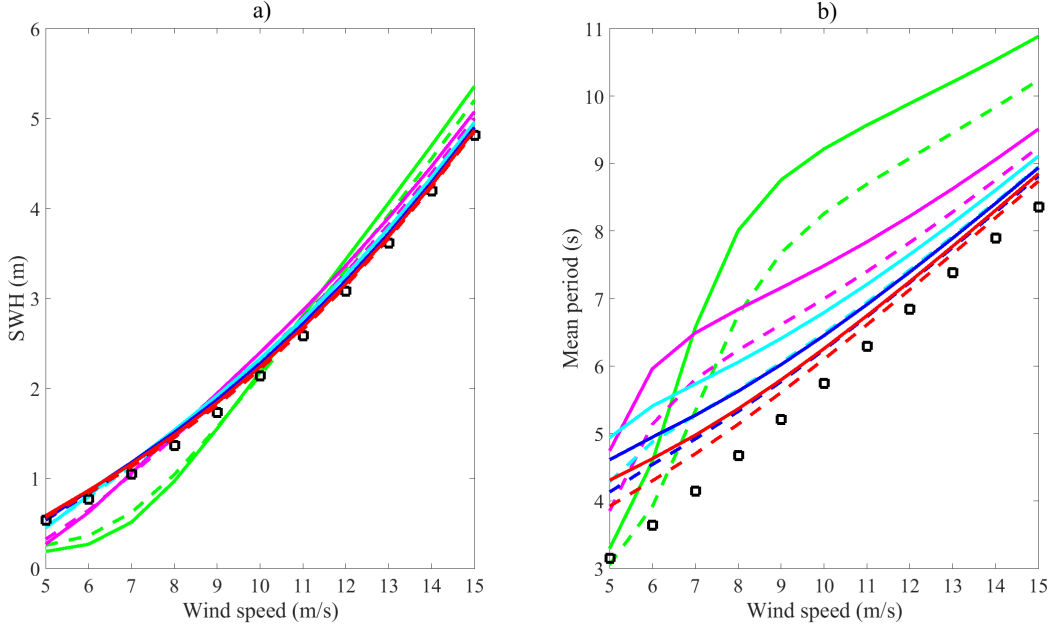


Fig. 3. Estimation of a) the SWH and b) the mean period from the Zeta function as a function of wind speed for a directional PM spectrum with the radar aiming in the upwind (solid lines) or crosswind (dashed lines) direction. The black squares show the theoretical value of the SWH and mean period. The various radar frequencies correspond to different color codes: 5 MHz (green); 10 MHz (magenta); 15 MHz (cyan); 20 MHz (red); 25 MHz (red).

is stronger than the negative frequency side) and take the following ratio

$$\Omega = \frac{\int_{\omega_B}^{+\infty} (\omega - \omega_B) \zeta(\omega) d\omega}{\int_{\omega_B}^{+\infty} \zeta(\omega) d\omega}. \quad (37)$$

After integration of the delta function this can be rewritten as

$$\Omega = \frac{\int (\omega_1 + \omega_2 - \omega_B) S_d(\mathbf{k}_1) S_d(\mathbf{k}_2) d\mathbf{k}_1}{\int S_d(\mathbf{k}_1) S_d(\mathbf{k}_2) d\mathbf{k}_1}. \quad (38)$$

Again, the leading contribution of the integrand occurs when one of the frequency k_1 or k_2 is close to zero and the other close to k_B , so that one of the ω_1, ω_2 variable cancel out with the $-\omega_B$ term. This identifies Ω as the centroid frequency

$$\Omega \simeq \frac{\int \omega(\mathbf{k}) S_d(\mathbf{k}) d\mathbf{k}}{\int S_d(\mathbf{k}) d\mathbf{k}} = \frac{2\pi}{T} \quad (39)$$

which defines the mean period T . We performed numerical simulations, shown in Fig. 3, to estimate the SWH and the mean wave period T from the Zeta function for the directional PM spectrum at various wind speed and direction at several radar frequencies covering the typical range of HF radars (from 5 to 25 MHz). We found that the SWH is increasingly well estimated by formula (35) as the radar frequency varies from 10 to 25 MHz but is poorly estimated at the lowest frequency (5 MHz). The same conclusion applies to the mean period, which is overestimated by formula (39-37) but becomes more accurate at higher radar frequencies and larger wind speed. This is consistent with the expectation that the approximation that was used to evaluate the integral of the Zeta function (34) necessitates a high ratio of the Bragg wavenumber k_B to the peak wavenumber k_p . The observed dependence of the estimated wave parameters on the radar frequency in Fig. (3)

TABLE I
CORRECTIVE FACTORS TO APPLY IN THE DERIVATION OF THE SEA STATE PARAMETERS FROM THE ZETA FUNCTION

Radar frequency (MHz)	10	15	20	25
α	0.93	0.95	0.96	0.97
T_0 (sec)	1.25	0.76	0.53	0.4

suggests that the estimated SWH (\hat{H}_s) should be corrected for by a multiplicative bias while the estimated mean period (\hat{T}) should be corrected for by an additive bias

$$\hat{H}_s \rightarrow \alpha \hat{H}_s, \quad \hat{T} \rightarrow \hat{T} - T_0. \quad (40)$$

By adjusting the average of the upwind and cross-wind estimation to the theoretical wave parameters for the ensemble of wind speeds we obtained parameters α and T_0 that depend on the sole radar frequency. These values are summarized in Table I. The corrective factor for the SWH ranges from 0.93 to 0.97 when increasing the radar frequency to 10 to 25 MHz (we discard the case 5 MHz) while the bias to subtract from the mean period ranges from 1.25 to 0.4 second.

IV. THE WEIGHTING FUNCTION

In order to make the expression of the ocean Doppler spectrum analytically tractable for sea state inversion, Barrick [8] proposed to replace the coupling coefficient $|\Gamma|^2$ by the so-called weighting function, obtained by performing an angular average $|\bar{\Gamma}|^2$ over the admissible wavenumbers

$$\frac{k_0^2}{8} \mathcal{W}_B(\nu) = |\bar{\Gamma}|^2. \quad (41)$$

We found this weighting function difficult to implement from the original publication and we used the numerical routine

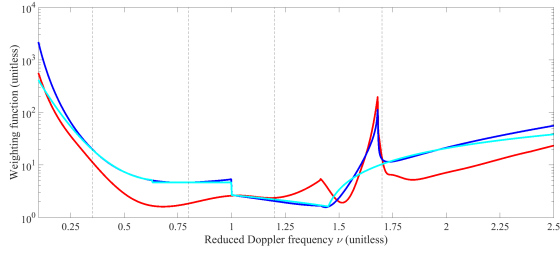


Fig. 4. New weighting function (blue solid line) as compared to Barrick's weighting function (red solid line). The simple analytical fit (46) is also shown (cyan line). The dashed vertical lines mark the 2 approximate frequency intervals ($[0.35 - 0.8]$ and $[1.2 - 1.7]$ where the weighting function is useful).

provided by the free RadarWIC library [13], that uses a digitized version of the Fig. 3 of [8]. Our reformulation of the second-order integral (12) suggests the construction of a different weighting function, using the same normalization factor as Barrick

$$\frac{k_0^2}{8} \mathcal{W}(\nu) = k_B^2 \langle \gamma \rangle_{I(\nu)} \quad (42)$$

where $\langle \gamma \rangle_{I(\nu)}$ is an average value of γ over the reduced frequency domain I_ν . For $\nu > 1$, this domain is narrow and it is justified to defined it with the mean value of the coupling coefficient over this interval

$$\langle \gamma \rangle_{I(\nu)} = \frac{\int_{I(\nu)} \gamma(\nu_1) d\nu_1}{\int_{I(\nu)} d\nu_1}, \quad \nu > 1. \quad (43)$$

For $0 < \nu < 1$, the values of both the kernel γ and the product of spectra in the integrands (19) are more contrasted, so that is not relevant to retain the mean value. However, we observed numerically and checked analytically that the integrand reach their dominant value at the edges of the integration domain. To give more weight to the latter, we replaced the mean by a simple 3 points average between the ends and the middle of the lower interval $I_{-1,1}(\nu)$ (we recall that the integral on the upper interval $I_{1,-1}(\nu)$ is identical)

$$\langle \gamma \rangle_{I(\nu)} = \frac{1}{3} \left(\gamma(A_\nu) + \gamma\left(\frac{A_\nu + B_\nu}{2}\right) + \gamma(B_\nu) \right) \quad (44)$$

with

$$A(\nu) = \frac{\nu^2 - 1}{2\nu}, \quad B(\nu) = \frac{\nu - \sqrt{2 - \nu^2}}{2}. \quad (45)$$

For $\nu < 0$, the weighting function is extended by parity (i.e., $\mathcal{W}(-\nu) = \mathcal{W}(\nu)$). Barrick's weighting function and ours are shown in Fig. 4. Both exhibit a singularity at $\nu = 2^{3/4}$ and follow the same trends but are quite different in magnitude. The difference in the definitions of the two weighting functions lies in the domain and variables of integration. Note that the new weighting function is no longer singular at $\nu = 2^{1/2}$ unlike Barrick's weighting function. This is because we do not include the Jacobian, which is at the origin of this singularity, in the definition. The new weighting function can be easily implemented from (43) and (45) but it is more convenient to have an analytical expression in the form of an empirical fit.

We found the following elementary linear fit, which is enough for our purposes

$$\mathcal{W}(\nu) = \begin{cases} \exp(13.87\nu^2 - 18.38\nu + 7.72) & \text{if } 0 < \nu < 0.63 \\ 4.64 & \text{if } 0.63 < \nu < 1 \\ -2.33\nu + 5 & \text{if } 1 < \nu < 1.45 \\ 34.87\nu - 48.93 & \text{if } \nu > 1.45. \end{cases} \quad (46)$$

To simplify the fit we did not retain the peak of the $2^{3/4}$ singularity, which has a negligible role in the integration of the Zeta function. Note also that the new weighting function has a discontinuity at $\nu = 1$, due to the adaptation of the definition of the mean kernel for $0 < \nu < 1$. However, this discontinuity has no consequence since the weighting function is only useful in two small intervals of frequencies lying on each side of the Bragg frequency, which are approximately $[0.35 - 0.8]$ and $[1.2 - 1.7]$. They correspond to the intervals where the Zeta function has non-negligible values (see Fig. 5).

Approximating the coupling coefficient with its average value in the expression (12) of the second-order Doppler spectrum leads to the following relation with the Zeta function

$$\zeta(\omega) \simeq 2^5 \frac{\sigma_2(\omega)}{\mathcal{W}(\omega/\omega_B)}. \quad (47)$$

The properties of the Zeta function therefore transfer to the ocean Doppler spectrum provided the weighting function approximation is sufficiently accurate. In particular this leads to the following formulas for the estimation of the SWH and mean period

$$(k_0 H_0)^2 = 2\alpha^2 \int_{-\infty}^{+\infty} R_{\mathcal{W}}(\omega) d\omega \quad (48)$$

and

$$T = \frac{2\pi \int_{\omega_B}^{+\infty} R_{\mathcal{W}}(\omega) d\omega}{\int_{\omega_B}^{+\infty} (\omega - \omega_B) R_{\mathcal{W}}(\omega) d\omega} - T_0 \quad (49)$$

where we define the ratio of the weighted second-order to first order Doppler spectrum following the notation of [14] as

$$R_{\mathcal{W}}(\omega) = \frac{\sigma_2(\omega)/\mathcal{W}(\omega/\omega_B)}{\int_{-\infty}^{+\infty} \sigma_1(\omega) d\omega}. \quad (50)$$

Apart from the corrective factors α and T_0 these expressions were already established by Barrick ((11) and (13) of [9]). Their accuracy is related, on one hand on the ability of the weighting function to recover the Zeta function (47), and on the other hand on the quality of the estimation (35), (37) and (40) based on the Zeta function. To elucidate these points, we performed numerical simulations at various wind speed and radar frequencies using the directional PM spectrum. Fig. 5 shows a comparison between the exact expression of the Zeta function and its approximation (47) at the radar frequency 16 MHz. We tested both Barrick's weighting function and the fitted version of the new weighting function (46). From a visual inspection (which is confirmed numerically) it is clear that the latter is in general more accurate, especially in the upwind direction. As a result, the estimation of the sea states parameters from the second-order Doppler spectrum (eqs. (48)-(49)) is improved when using this new weighting

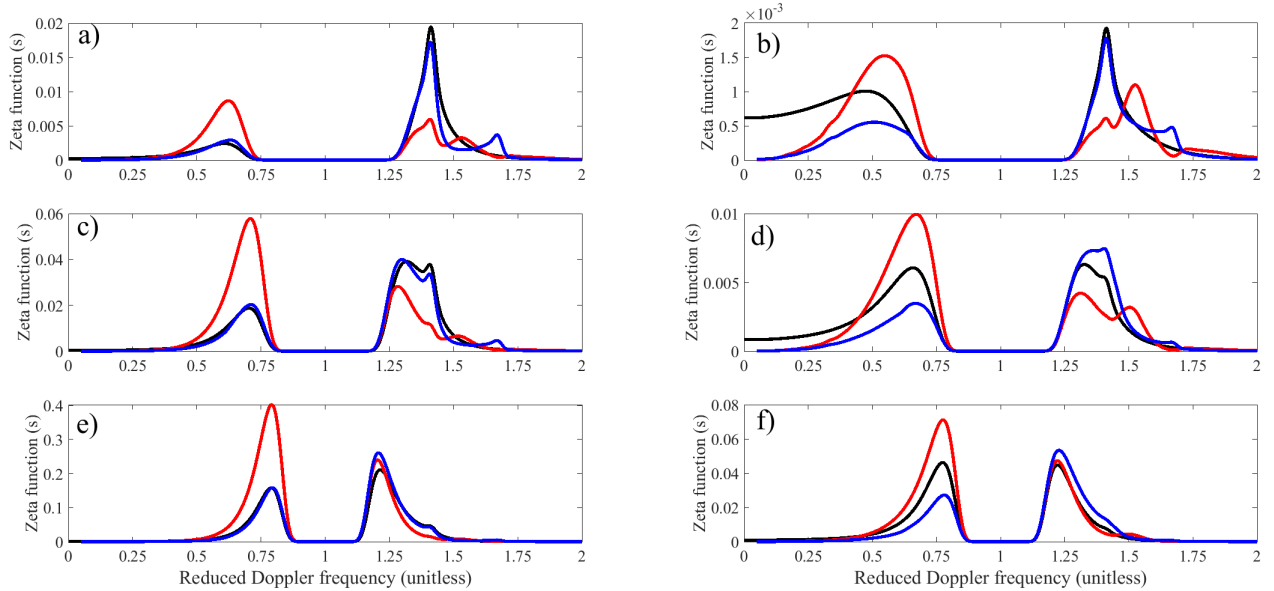


Fig. 5. Comparison of the Zeta function (black lines) and its evaluation with the ocean Doppler spectrum (47) using Barrick's weighting function (red line) and ours with the simple fit (46) (blue lines). The ocean Doppler spectrum was simulated at the radar frequency 16 MHz using an upwind directional PM spectrum by a) 7 m/s; c) 10 m/s; e) 15 m/s wind speed, and a crosswind directional PM spectrum by b) 7 m/s; d) 10 m/s; f) 15 m/s wind speed. The three functions have been smoothed with a window of width 0.01 Hz and are shown in linear scale (i.e., not dB) to highlight the frequency intervals where it the are non negligible.

function, even in its elementary fitted version (46). Fig. 6 shows the percentage of error between the estimated and actual values of the SWH and mean period as a function of dimensionless parameter $k_0 H_s$ for a directional PM wave spectrum at various wind speeds and radar frequencies. For reference, the result of the bias-corrected estimation with the Zeta function (eqs (35), (37) and (40)) is also shown. An overall error reduction is obtained with the new weighting function for $k_0 H_s > 0.5$. However, as already noted by other authors (e.g. [15]), inconsistent estimations are obtained in the upwind and crosswind direction; their discrepancy is reduced when using the new weighting function but remains, at best, of the order of 9% of the SWH for $k_0 H_s > 0.5$ and can reach 25% for $k_0 H_s < 0.5$ while it is of the order of 10% for the mean period. As seen, there is also a small discrepancy between the upwind and crosswind estimation from the Zeta function, especially for lower values of $k_0 H_s$ and for the mean period.

Note that an empirical correction (48) for the SWH arising from Barrick's formula has already been employed by several authors to improve its consistency with High-Frequency radar measurements [16]–[18]. At a radar frequency of 25.4 MHz, [18] found the best fit with $\alpha \simeq 0.58$ and [16] with $\alpha \simeq 0.55$. However, our value $\alpha = 0.97$ at 25 MHz has been obtained from the Zeta function and not from its approximation (47) with the weighting function, which can explain the difference.

V. A DIRECT RELATION TO THE WAVE SPECTRUM

In a series of papers [14], [19]–[21], attempts were made to find a simple linear relationship between the ocean wave spectrum and the second-order Doppler spectrum shift by the

Bragg frequency, as originally proposed by [3]. An empirical relation of the type

$$k_0^2 S_f(\omega) = 2A(\omega)R_{\mathcal{W}}(\omega \pm \omega_B) \quad (51)$$

which can be seen as the spectral form of Barrick's formula (48), has been sought with a frequency-dependent calibration coefficient $A(\omega)$ and different weighting functions (taken to be one for [19], [20] and adapted to wind-waves and swell for [14], [21]). Even though this method has shown good results when employed with experimental data, it is not fully satisfactory as it requires manual calibration for each radar site and bearing and is limited to the range of frequencies where the second-order Doppler spectrum can be linearized, i.e. not too far from the Bragg frequency. We propose here a nonlinear approximation, inspired by the reformulation (12) of the second-order Doppler spectrum as a frequency integral over the variable domain $I(\nu)$. For $|\nu| > 1$, the integration domain $I(\nu)$ is narrow (see Fig. 1) and we can therefore approximate the above integral by extracting the mean value $\bar{\mathcal{S}}$ of the function \mathcal{S} over this interval, leading to

$$\sigma_2(\omega) \simeq \mathcal{N} k_B^4 \omega_B^{-1} \bar{\mathcal{S}}(\nu) \mathcal{F}(\nu) \quad (52)$$

where

$$\mathcal{F}(\nu) = \int_{I(\nu)} \gamma(\nu_1) \mathcal{J}(\nu_1) d\nu_1 \quad (53)$$

is a deterministic function that does not depend on sea state nor on the radar frequency and can thus be calculated once for all. This function, which is shown in Fig. 7, carries the 2 singularities at $\nu = 2^{1/2}$ and $\nu = 2^{3/4}$ but has otherwise a

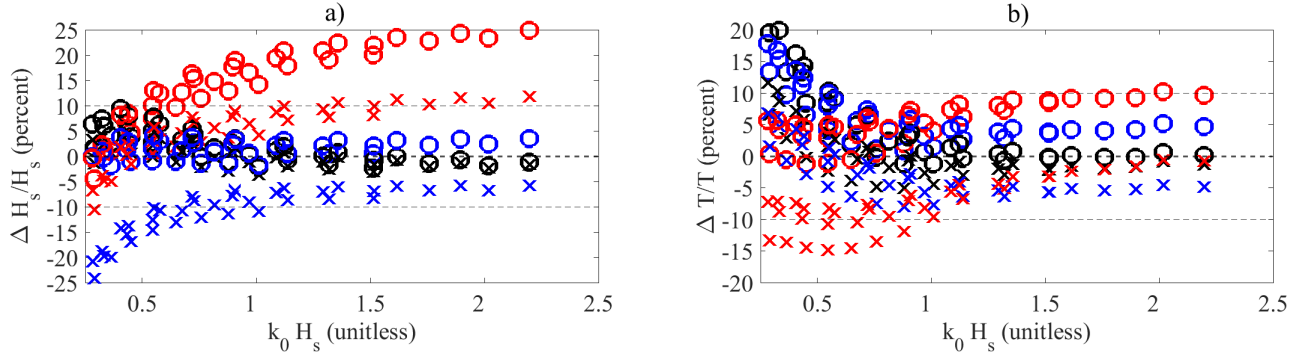


Fig. 6. Relative error (in percent) in the estimation of a) the SWH and b) the mean period from the second-order Doppler spectrum (eqs. (48)-(49)) using either Barrick's weighting function (red symbols) or fitted weighting function (46) (blue symbols). The errors are shown as a function of the dimensionless roughness parameter $k_0 H_s$, wherein the results of the four frequency bands 10,15,20 and 25 MHz have been concatenated. The estimation based on the Zeta function is shown for reference in black symbols. The circles correspond to the upwind direction and the crosses to the crosswind direction.

smooth polynomial behavior. For $\nu > 1.7$ it can be described by the following fit with an excellent accuracy

$$\mathcal{F}(\nu) = 0.0592\nu^3 - 0.2935\nu^2 + 0.5038\nu - 0.2958. \quad (54)$$

To obtain a tractable expression we define \bar{S} in the following

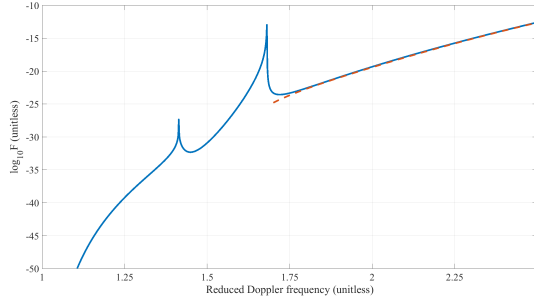


Fig. 7. Function $\mathcal{F}(\nu)$ (blue solid line) as defined in (53) and expressed in decibels, together with its fit (54) for $\nu > 1.7$ (dashed red line).

way. For $1 \leq \nu \leq \sqrt{2}$, the integration domain $I(\nu)$ consists of 2 narrow intervals given by (18) and we may approximate \mathcal{S} by its average between the endpoints of each interval; for $\nu > \sqrt{2}$, the integration domain $I(\nu)$ consists of a single wider interval on which we may approximate \mathcal{S} by its average between the midpoint and the endpoints. Altogether, this leads to the following definition

$$\bar{S}(\nu) = \begin{cases} \frac{1}{4}(S_1^+ + S_1^- + S_2^+ + S_2^-), & \text{if } 1 \leq \nu \leq \sqrt{2} \\ \frac{1}{4}(2S_0 + S_2^+ + S_2^-), & \text{if } \nu > \sqrt{2} \end{cases} \quad (55)$$

with

$$S_0 = \mathcal{S}(\nu/2), \quad S_1^\pm = \mathcal{S}\left(\frac{\nu \pm \sqrt{2 - \nu^2}}{2}\right), \quad S_2^\pm = \mathcal{S}\left(\frac{\nu^2 \pm 1}{2\nu}\right). \quad (56)$$

From the relation (29) we can convert this last expression in terms of directional frequency spectrum

$$\begin{aligned} S_0 &= \frac{32g^4}{\omega^6} S_f^2(\omega/2) (D(\omega/2, \theta_0) D(\omega/2, -\theta_0)), \\ S_1^\pm &= \frac{32g^4}{(\omega_1^+ \omega_1^-)^3} S_f(\omega_1^-) S_f(\omega_1^+) D(\omega_1^+, 0) D(\omega_1^-, 0) \\ S_2^\pm &= \frac{32g^4}{(\omega_2^+ \omega_2^-)^3} S_f(\omega_2^-) S_f(\omega_2^+) D(\omega_2^+, 0) D(\omega_2^-, 0) \\ \omega_1^\pm &= \frac{\omega \pm \sqrt{2\omega_B^2 - \omega^2}}{2}, \quad \omega_2^\pm = \frac{\omega^2 \pm \omega_B^2}{2\omega} \\ \theta_0 &= \text{atan}\left(\frac{1}{2}\sqrt{\frac{\omega^4}{\omega_B^4} - 4}\right). \end{aligned} \quad (57)$$

Similar relations hold for negative frequencies ($\nu < -1$), with the argument of the spreading function shifted by π ($D(\omega/2, \pm\theta_0) \rightarrow D(|\omega|/2, \pm\theta_0 + \pi)$, $D(\omega_{1,2}^\pm, 0) \rightarrow D(|\omega_{1,2}^\pm|, \pi)$). Fig. 8 shows a comparison of the exact formula (12) and its approximated version using (52) for a PM spectrum by 10 m/s wind speed for an upwind looking radar at 16 MHz. We found the approximation good for $\nu > 1.5$ (less than 2 dB error) and excellent for $\nu > 1.75$ (less than 0.5 dB error). We checked numerically other wind speeds and radar frequencies with the same conclusion. This formula shows that starting from $\omega = 2^{1/2}\omega_B$, the part of the ocean wave frequency spectrum that contributes to the Doppler spectrum at a given Doppler frequency ω is a narrow interval around $\omega/2$. The directions of waves involved in this process are those having an angle smaller than θ_0 with respect to the radar beam. This last angle is null at $\omega = 2^{1/2}\omega_B$, reaches 45 degree at $2^{3/4}\omega_B$, and 60 degree at $2\omega_B$ and converges to the cross-beam directions 90 degree as the frequency keeps increasing. Note that in the vicinity of the first singularity $2^{1/2}\omega_B$, the angle θ_0 is close to zero so that the radar dominantly "sees" the waves that are propagating along or against the radar look direction.

VI. CONCLUSION

We have proposed a formulation of the second-order ocean Doppler spectrum based on an integration of the sole fre-

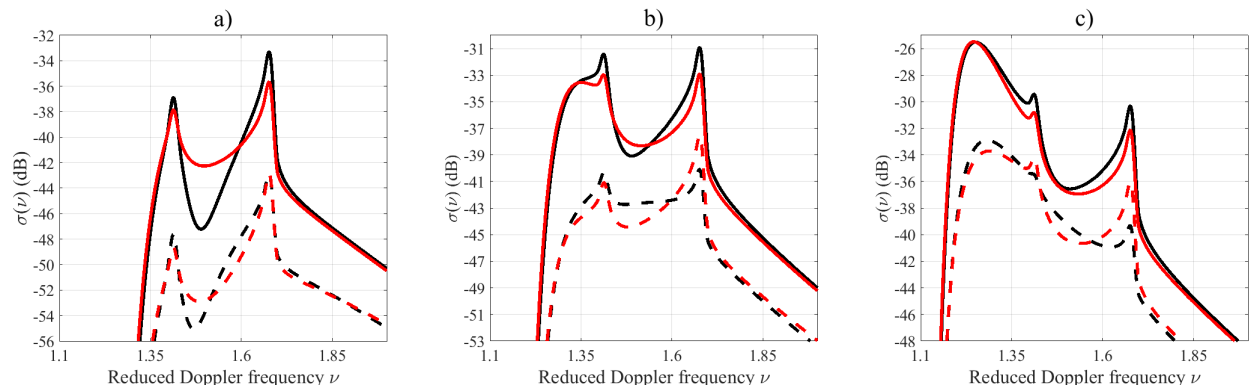


Fig. 8. Exact numerical calculation (black lines) of the second-order Doppler spectrum compared with its analytical approximation with s (52) (red lines) for a directional PM spectrum. The radar is looking upwind (solid lines) or crosswind (dashed lines) at 16 MHz and the wind speed is a) 7 m/s; b) 10 m/s; c) 15 m/s.

quency variable. This new expression allows for efficient and accurate numerical evaluation of the Doppler spectrum. In addition, it leads naturally to an alternative weighting function that can be used to improve the estimation of the main sea state parameters after the classical method proposed by Barrick in 1977 ([8], [9]) and reduces the discrepancy between the upwind and crosswind estimation. Nevertheless, there are some limitations to this method, which are not related to the quality of the weighting function but to the structure of the Zeta function. A bias correction for both the SWH and mean period is necessary, with values depending on the radar frequency, and there remains a small but non negligible discrepancy between the upwind and crosswind estimation from a single radar site. A second important consequence of our approach is the derivation of an analytical nonlinear approximation for the ocean wave spectrum for Doppler frequencies well beyond the Bragg frequency. This formula might be a useful complement to classical techniques of ocean wave spectrum inversion which are often limited to the frequencies close to the Bragg frequency (typically in the range $0.4 < \nu < 1.6$) where the problem can be linearized (see e.g. the discussions in [4] or [15]).

Acknowledgments: This research has been funded by the Agence Nationale de la Recherche (ANR) under grant ANR-22-ASTR-0006-01 (ROSMED project: “Radar à Ondes de Surface en MEDiterranée”)

REFERENCES

- [1] Pablo Lorente et al., “Coastal high-frequency radars in the Mediterranean - Part 1: Status of operations and a framework for future development,” *Ocean Science*, vol. 18, pp. 761–795, 2022.
- [2] D E Barrick, “Remote sensing of sea state by radar,” in *Remote sensing of the Troposphere*. 1972, vol. 12, pp. 1–46, VE Derr, Editor, US Government, Publisher: Washington, DC: US Government Printing Office.
- [3] Klaus Hasselmann, “Determination of ocean wave spectra from doppler radio return from the sea surface,” *Nature Physical Science*, vol. 229, no. 1, pp. 16–17, 1971.
- [4] Lucy R Wyatt, “Limits to the inversion of HF radar backscatter for ocean wave measurement,” *Journal of Atmospheric and Oceanic Technology*, vol. 17, no. 12, pp. 1651–1666, 2000.
- [5] Belinda Lipa, “Derivation of directional ocean-wave spectra by integral inversion of second-order radar echoes,” *Radio Science*, vol. 12, no. 3, pp. 425–434, 1977.
- [6] L Wyatt, “A relaxation method for integral inversion applied to HF radar measurement of the ocean wave directional spectrum,” *Int J Remote Sens*, vol. 11, no. 8, pp. 1481–1494, 1990.
- [7] Yukiharu Hisaki, “Nonlinear inversion of the integral equation to estimate ocean wave spectra from HF radar,” *Radio science*, vol. 31, no. 1, pp. 25–39, 1996.
- [8] Donald E Barrick, “The ocean waveheight nondirectional spectrum from inversion of the HF sea-echo Doppler spectrum,” *Remote Sensing of Environment*, vol. 6, no. 3, pp. 201–227, 1977, Publisher: Elsevier.
- [9] Donald E Barrick, “Extraction of wave parameters from measured HF radar sea-echo Doppler spectra,” *Radio Science*, vol. 12, no. 3, pp. 415–424, 1977, Publisher: AGU.
- [10] B J Lipa and D E Barrick, “Extraction of sea state from HF radar sea echo: Mathematical theory and modeling,” *Radio Science*, vol. 21, no. 1, pp. 81–100, 1986, Publisher: Wiley Online Library.
- [11] J Walsh and EW Gill, “An analysis of the scattering of high-frequency electromagnetic radiation from rough surfaces with application to pulse radar operating in backscatter mode,” *Radio Science*, vol. 35, no. 6, pp. 1337–1359, 2000.
- [12] Dmitry V Ivonin, Victor I Shrira, and Pierre Broche, “On the singular nature of the second-order peaks in HF radar sea echo,” *IEEE Journal of Oceanic Engineering*, vol. 31, no. 4, pp. 751–767, 2006.
- [13] Douglas Cahl, George Voulgaris, and Zaid Alattabi, “Wave radar inversion code (waveric) v1.0.1 (version v1.0.1),” <http://doi.org/10.5281/zenodo.2643696>, April 2019.
- [14] Zaid R Alattabi, Douglas Cahl, and George Voulgaris, “Swell and wind wave inversion using a single very high frequency (VHF) radar,” *Journal of Atmospheric and Oceanic Technology*, vol. 36, no. 6, pp. 987–1013, 2019.
- [15] L. Wyatt, *Ocean Remote Sensing Technologies—High-Frequency, Marine and GNSS-Based Radar*, edited by Huang, Weimin and Gill, Eric W, chapter Ocean wave measurement, pp. 145–178, SciTech Publishing Raleigh, NC, USA, 2021.
- [16] SF Heron and ML Heron, “A comparison of algorithms for extracting significant wave height from HF radar ocean backscatter spectra,” *Journal of Atmospheric and oceanic technology*, vol. 15, no. 5, pp. 1157–1163, 1998.
- [17] Joseph W Maresca Jr and TM Georges, “Measuring rms wave height and the scalar ocean wave spectrum with HF skywave radar,” *Journal of Geophysical Research: Oceans*, vol. 85, no. C5, pp. 2759–2771, 1980.
- [18] Rafael J Ramos, Hans C Graber, and Brian K Haus, “Observation of wave energy evolution in coastal areas using HF radar,” *Journal of atmospheric and oceanic technology*, vol. 26, no. 9, pp. 1891–1909, 2009.
- [19] Klaus-Werner Gurgel, Heinz-Hermann Essen, and Thomas Schlick, “An empirical method to derive ocean waves from second-order Bragg scattering: Prospects and limitations,” *IEEE Journal of Oceanic Engineering*, vol. 31, no. 4, pp. 804–811, 2006, Publisher: IEEE.
- [20] Guiomar Lopez, Daniel C Conley, and Deborah Greaves, “Calibration, validation, and analysis of an empirical algorithm for the retrieval of wave spectra from HF radar sea echo,” *Journal of Atmospheric and Oceanic Technology*, vol. 33, no. 2, pp. 245–261, 2016.
- [21] Zaid R Al-Attabi, George Voulgaris, and Daniel C Conley, “Evaluation and validation of HF radar swell and wind-wave inversion method,” *Journal of Atmospheric and Oceanic Technology*, vol. 38, no. 10, pp. 1747–1775, 2021.